Title: Hydrodechlorination and complete degradation of chlorinated compounds with the coupled action of Pd/SiO_2 and Fe/SiO_2 catalysts: towards industrial catalyst synthesis conditions

Authors: Julien G. Mahy, Ludivine Tasseroul, Olivier Tromme, Benoît Lavigne, Stéphanie D. Lambert

PII: S2213-3437(19)30137-X
DOI: https://doi.org/10.1016/j.jece.2019.103014
Article Number: 103014

Reference: JECE 103014

To appear in:

Received date: 11 January 2019
Revised date: 26 February 2019
Accepted date: 9 March 2019

Please cite this article as: Mahy JG, Tasseroul L, Tromme O, Lavigne B, Lambert SD, Hydrodechlorination and complete degradation of chlorinated compounds with the coupled action of Pd/SiO_2 and Fe/SiO_2 catalysts: towards industrial catalyst synthesis conditions, *Journal of Environmental Chemical Engineering* (2019), https://doi.org/10.1016/j.jece.2019.103014

Hydrodechlorination and complete degradation of chlorinated compounds with the coupled action of Pd/SiO_2 and Fe/SiO_2 catalysts: towards industrial catalyst synthesis conditions

Julien G. Mahy[1*], Ludivine Tasseroul[1], Olivier Tromme[2], Benoît Lavigne[2], Stéphanie D. Lambert[1]

[1] *Department of Chemical Engineering – Nanomaterials, Catalysis & Electrochemistry, University of Liège, B6a, Quartier Agora, Allée du six Août 11, 4000 Liège, Belgium*

[2] *Sanifox SPRL, Rue Enhet-Centre 47, 5590 Chevetogne, Belgium*

***Corresponding author:** Julien G. Mahy, , Department of Chemical Engineering – Nanomaterials, Catalysis & Electrochemistry, University of Liège, B6a, Quartier Agora, Allée du six Août 11, 4000 Liège, Belgium. E-mail address: julien.mahy@uliege.be. Tel: +32 4 366 35 63.

Graphical abstract

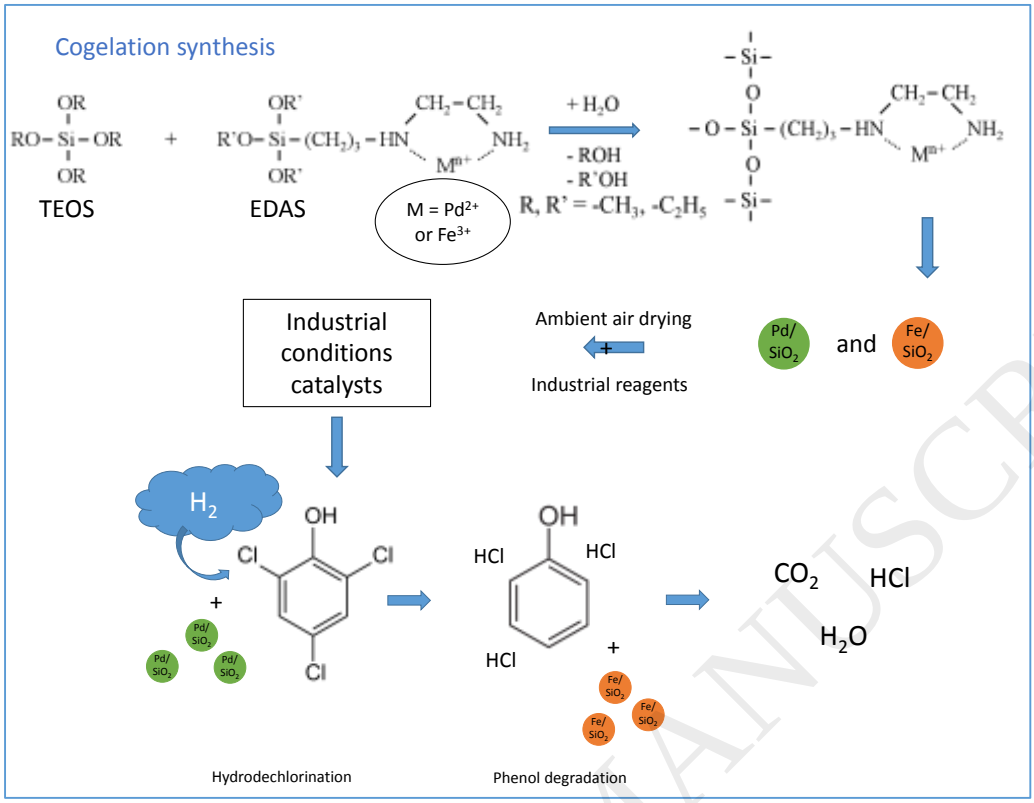

Highlights

- Binary Pd/SiO_2 and Fe/SiO_2 catalysts synthesized by the cogelation process
- Study of the scaling-up of the synthesis method for catalysts
- Metallic species highly dispersed in silica matrix
- Efficient catalysts for the hydrodechlorination and degradation of trichlorophenol

Abstract

In this study, Pd/SiO_2 and Fe/SiO_2 catalysts have been synthesized by the cogelation process for hydrodechlorination applications. Different synthesis conditions were tested to approach the

industrial conditions using industrial grade reactants and ambient air drying. The influence of these changes have been studied on the texture and the catalytic activity of the catalysts. The resulting materials are composed of metallic (Pd catalysts) or metallic oxide (Fe catalysts) nanoparticles highly dispersed in porous silica. The catalysts present a high specific surface area (between 250 and 500 m^2/g) with a large pore size range between micro-, meso- and macropores. The modifications of the synthesis conditions give catalysts with similar textural properties compared to lab-scale catalysts. The catalytic activity of the binary catalysts have been evaluated on the hydrodechlorination of the *2,4,6*-trichlorophenol (TCP) in water. Results show that Pd/SiO_2 catalysts are able to dechlorinate the TCP and that Fe/SiO_2 materials are able to degrade the resulting phenol. So this process allows a complete degradation of TCP. Industrial conditions catalysts show also similar catalytic results compared to lab-scale catalysts for the hydrodechlorination of the 2,4,6-trichlorophenol (TCP) in water.

Keywords: Cogelation process, *2,4,6*-trichlorophenol degradation, hydrodechlorination, Pd/SiO_2, Fe/SiO_2

1. Introduction

Chlorophenols are toxic molecules usually used as intermediates for organic synthesis, pesticides, herbicides or disinfectant [1–3]. These molecules are persistent, carcinogenic and can be found in the environment as residual pollutant in water, soil and even in air [1–3].

Due to environmental legislations [1,2,4] and in order to keep healthy environment, it is necessary to dechlorinate and degrade these molecules in waste water effluents.

Several methods have been developed for treating chlorophenol-contaminated water [2], as thermal treatment, sonification, ozonation, electrochemical treatment, Fenton-type oxidative degradation [5], advanced oxidation, photocatalysis, bioremediation [6], reductive

dechlorination by zero valence metals [4] and bimetallics [7,8], adsorption on diversified materials, electrocatalytic reduction [3], and catalytic hydrodechlorination (HDC) [2].

The catalytic hydrodechlorination have paid particular attention these past years [9–13] with the development of numerous catalysts. The reactions often consists of the hydrogenolysis between carbon and chloride atom [9] (equation 1).

$$\equiv C–Cl + H_2 \rightarrow \equiv C– H + HCl \quad (1)$$

In equation 1, hydrogen atoms are substituted for chlorine atoms. Noble metal catalysts (Group VIII) are very active for the hydrodechlorination reaction [9,14]. Among noble metals, palladium (Pd) is one of the most efficient catalyst for hydrodechlorination [1,2,8]. These catalysts are very effective but also very expensive, so the development of catalyst needs to maximize the efficiency while limiting the amount of noble metal. It is often dispersed on a support, like silica [9,15], carbon [2,16], alumina [13] or zeolithe [17], to limit its loading . Different syntheses are previously developed as impregnation of support [16], sol-gel process [9,15] or reduction method [18]. Sol-Gel process has shown a method for dispersing metallic nanoparticles inside a metal oxide matrix, as silica, thanks to modified alkoxides able to form complexes with metallic precursor [11,15,19]. This method was called cogelification [15]. Indeed, in different fields, the sol-gel method has been used successfully in order to highly disperse metallic nanoparticles in an inorganic matrix and it has been tested with a good response as show in [20,21].

In the major studies about dechlorination, chlorinated compounds were converted in HCl and hydrogenated compounds, as phenol, that needed supplementary treatment to be eliminated [2,4].

Moreover, the developed catalysts are mainly synthesized in laboratory scale with high purity reactants far different from industrial conditions [2,4].

In this work, the aim will be to develop, with the cogelation process, binary catalysts able to completely degrade chlorinated compounds. For the hydrodechlorination step, Pd/SiO_2 catalysts will be synthesized and for the degradation of hydrogenated compounds step, Fe/SiO_2 catalysts will be developed. The catalyst synthesis will be develop at laboratory scale, then will be modify to reach closer industrial conditions by using industrial grade reactants and ambient air drying. The catalysts will be characterized by nitrogen adsorption-desorption isotherm measurements, transmission electron microscopy, mercury porosimetry measurement, Mössbauer spectroscopy or x-ray diffraction to assess the impact of condition modifications towards industrial scale. The catalytic activity will be assessed on the complete degradation of *2,4,6*-trichlorophenol (TCP, 98%, Sigma Aldrich). A mechanism of complete degradation of TCP with the two catalysts will be proposed.

2. Materials and methods

2.1.1. Gel synthesis

Synthesis operating variables for the samples are given in Table 1. Three iron xerogel catalysts and three palladium catalysts were prepared by the cogelation method with three different conditions of synthesis: classical method (named -C), industrial 1 (named -I1) and industrial 2 (named -I2). Same percentage of metals (1 wt%) were added in samples.

For the "classical method", two samples (one with Fe and one with Pd) [22,23] were prepared in absolute ethanol (Merck, > 99 %) with the iron precursor, $Fe(acac)_3$ (Fe(III) acetylacetonate, $Fe(CH_3C(O)CH(O\text{-})CH_3)_3$, Aldrich, 97 %) or with the palladium precursor, $Pd(acac)_2$, (palladium acetylacetonate, $Pd(CH_3COCH{=}C(O\text{-})CH_3)_2$, Aldrich, 97 %), TEOS (tetraethoxysilane, $Si(OC_2H_5)_4$, Aldrich, 98 %), EDAS (*3*-(*2*-

aminoethylamino)propyltrimethoxysilane, $(CH_3O)_3Si(CH_2)_3NH(CH_2)_2NH_2$, Merck, 97 %) and 0.54 M of NH_3 aqueous solution. For both synthesis, $Fe(acac)_3$ or $Pd(acac)_2$ was mixed with EDAS in half of the total volume of ethanol. The mixture is stirred at room temperature until the metallic precursor has completely dissolved to produce a colored solution (about 1 h). After addition of TEOS, a 0.54 M NH_3 aqueous solution in the remaining half of the total ethanol volume was added to the mixture under vigorous stirring. The volume of the final solutions was about 220 mL.

For gelation and ageing, the sample vessel was sealed and heated to 80 °C for 72 h. The gel time of each sample is determined visually: the glass bottle is tilted at 45°, and if the sample no longer flows, it is considered gelled. The different molar ratio used to calculate the amount of reactants are the hydrolysis ratio, *i.e.*, $[H_2O]/([TEOS] + ¾ [EDAS])$, and the dilution ratio, *i.e.*, $[H_2O]/([TEOS] + [EDAS])$, equal to 5 and 10 respectively. The scheme of the synthesis is depicted in Figure 1.

After 72 h at 80 °C, the gels were dried under vacuum by placing the open vessel in an oven at 80 °C. The pressure was slowly decreased (to prevent gel bursting) to a minimum of 1000 Pa after 120 h. The samples were then heated at 150 °C for 72 h at 1000 Pa. The resulting samples are xerogels [24]. The two samples were called Fe/SiO_2-C and Pd/SiO_2-C

In order to transfer the synthesis towards industrial scale, similar syntheses were made with industrial conditions.

For the “industrial 1” way, two samples were also prepared with industrial grade reagents: Dynasil (ABCR, 78-10-4) replaced TEOS and Dynasilan DAMO (ABCR, 1760-24-3) replaced EDAS. The same step as previous paragraphs were realized. The two samples were called Fe/SiO_2-I1 and Pd/SiO_2-I1.

For the last synthesis method, called “industrial 2”, two samples were synthesized with industrial grade reagents (Dynasil and Dynasilan) again but this time, the vacuum drying step

is replaced by an ambient following air drying of 12 h in order to reduce the time of drying and to save energy. The other steps are identical to the first method. The two samples were called Fe/SiO_2-I2 and Pd/SiO_2-I2.

2.2. Calcination

All the samples were heated up to 450 °C at a rate of 120 °C h^{-1} under flowing air (9 NL h^{-1}) at atmospheric pressure and maintained at this temperature for 8 h. Then, they were again heated up to 550 °C at a rate of 120 °C h^{-1} under flowing air (9 NL h^{-1}) at atmospheric pressure and maintained at this temperature for 4 h.

2.3. Reduction

Only for the Pd-doped series, the samples were reduced under H_2 for 3 h at 350°C.

2.4. Sample characterization

Apparent densities, ρ_{app}, were measured by helium pycnometry by using a Micromeritics AccuPyc 1330 device. Nitrogen adsorption-desorption isotherms were measured at 77 K in an ASAP 2420 multi-sampler adsorption-desorption volumetric device from Micromeritics. Mercury porosimetry measurements were performed between 0.01 and 200 MPa by using two Thermo Scientific Pascal 140 and 240 devices. Nitrogen adsorption-desorption isotherms provided the specific surface area by the BET method, S_{BET}, the specific mesopore surface area determined by the Broekhoff–de Boer theory, S_{BdB}, the specific mesopore volume determined by the Broekhoff–de Boer theory, $V_{cum<7.5nm}$, the specific micropore volume calculated by Dubinin-Radushkevich theory, V_{DR}, and the specific liquid volume adsorbed at saturation pressure of nitrogen, V_P [25]. Mercury porosimetry measurements provided the specific

macropore volume, V_{HG} [26]. The combination of nitrogen adsorption-desorption isotherms and mercury porosimetry is used to calculate the pore size distribution [22].

Percentages of iron and palladium in the samples were determined by inductively coupled plasma–atomic emission spectroscopy (ICP–AES), equipped with an ICAP 6500 THERMO Scientific device [23]. Solutions for analysis were prepared as follows [23]: (i) 2 g of Na_2O_2, 1 g of NaOH and 0.1 g of sample were mixed in a vitreous carbon crucible; (ii) the mixture was heated beyond the melting point (up to 950 °C); (iii) after cooling and solidification, the mixture was digested in 30 mL of HNO_3 (65%); (iv) the solution was then transferred into a 500 mL calibrated flask that was finally filled with deionized water [23].

The size of iron oxide, palladium and silica nanoparticles was measured by transmission electron microscopy (TEM) by using a Phillips CM 100 device. First, samples were dispersed in absolute ethanol using an ultrasonic treatment. Then a drop of the dispersion was placed on a copper grid (Formvar/Carbon 200 Mesh Cu from Agar Scientific).

X-ray diffraction-patterns were recorded with a Bruker D8 Twin-Twin powder diffractometer using Cu-K_α radiation. The sizes of the metallic species crystallites, d_{XRD}, are estimated from XRD measurements by the Scherrer method [27]:

$$d_{XRD} = 0{,}9\frac{\lambda}{B\ \cos\theta} \qquad (2)$$

where B is the full-width at half-maximum after correction of the instrumental broadening, λ is the wavelength (nm), θ is the Bragg angle (rad) [28,29].

Mössbauer spectra were obtained on a constant acceleration spectrometer at 295 K with a cobalt-57 source calibrated with α–iron foil.

2.5. Hydrodechlorination of *2,4,6*-trichlorophenol in water

Hydrodechlorination of *2,4,6*-trichlorophenol (TCP) by Pd/SiO_2 and Fe/SiO_2 catalysts was realized in glass bottles of 270 mL containing 200 mL of deionized water with 50 ppm of TCP. The concentration in catalyst was 10^{-4} M for the Fe-doped SiO_2 samples and 10^{-5} M for the Pd-doped SiO_2 samples.

The bottles were swept by a gas composed of 80 % of H_2 and 20% of CO_2 and they were stirred at 30 °C. The H_2 amount in the bottles was $2*10^{-3}$ moles. Sampling were made after 0, 2, 4, 6 and 24 h and TCP and phenol (POH) were dosed by HPLC to assess the remaining concentrations. Blank measurements without catalyst were made as references.

All the tested conditions are depicted in Table 2, each pair (Fe- and Pd-doped SiO_2 samples) synthesized by one of the three ways of synthesis was tested with the test plan of Table 2. Each condition is made in triplicate.

In order to ensure the complete mineralization of the pollutant with the catalytic experiments, total organic carbon (TOC) measurements have been performed using a Hach DRB200 Reactor and a Total Organic Carbon Direct Method Test N Tube™ Reagent Set [30]. The TOC is determined by first sparging the sample under slightly acidic conditions to remove the inorganic carbon [30]. In an outside vial, the organic carbon contained in the sample is digested by persulphate and acid to form carbon dioxide. During digestion, the carbon dioxide diffuses into a pH indicator reagent in an inner ampoule [30]. The adsorption of carbon dioxide into the indicator forms carbonic acid. Carbonic acid influences the pH of the indicator solution which, in turn, changes the color. The amount of color change is related to the original amount of carbon present in the sample and can be evaluated using a Hach DR 2800 Spectrophotometer at 430 nm [30].

3. Results

3.1.Sample composition and morphology

Theoretical and actual loadings of palladium and iron are similar for all samples (Table 1).

XRD patterns, obtained for all calcined iron xerogel catalysts, show no characteristic iron species peaks (Figure 2), and identification of the iron species present in the xerogels is not possible from this data as previously shown with this type of materials [23]. Concerning Pd series, the XRD patterns of Pd/SiO_2-I2 sample before and after reduction are depicted in Figure 2, the patterns for the 2 other samples are similar. The calcined and reduced Pd/SiO_2-I2 samples show a peak around 33.6° and 39.8° respectively, corresponding to palladium oxide and metallic palladium respectively. The size of metallic particles, d_{XRD}, is calculated thanks to Scherrer equation (2) giving nanoparticles around 3 and 2 nm respectively. The values of d_{XRD}, are presented in Table 3 for Pd series after reduction.

Figure 3 shows TEM micrograph for the Fe/SiO_2-C, Fe/SiO_2-I2, Pd/SiO_2-C and Pd/SiO_2-I2 samples. The largest particles, with sizes of about 15 to 30 nm (Table 3), correspond to silica particles. For Fe doped samples (Figure 3 A and B), small nanoparticles, with sizes of about 1 to 1.5 nm (Table 3), are located inside the silica particles as observed on Figure 3. For Pd-doped samples (Figure 3 C and D), palladium nanoparticles are observed inside silica particles, the size is around 2-3 nm. Their sizes are quite similar to the size of metallic particles, d_{XRD}, calculated by XRD pattern (Table 3). In this study, the sizes of metallic Pd nanoparticles obtained by TEM and XRD measurements are similar, highlighting the fact that the distribution of Pd nanoparticules sizes is very narrow and centered around 2-3 nm [22, 31].

Concerning Fe/SiO_2 catalysts, the Mössbauer spectroscopy is the most adapted technique to obtain information about iron. These samples have been measured previously in

Mahy *et al.* [23]. The Mössbauer spectrum of Fe/SiO_2-I2 sample, shown in Figure 4 as an example for all Fe/SiO_2 samples, presents an asymmetric broad doublet (grey fitted line on Figure 4), which is the combination of two signals: (i) the first one, composed of a asymmetric doublet with an average isomer shift of 0.30(2) mm/s and an average quadrupole splitting of 1.0(1) mm/s depicted in red in Figure 4 and (ii) a second component, corresponding to a broad single line, depicted in blue in Figure 4, with a linewidth of 4 mm/s and an isomer shift of 0.3 mm/s. This decomposition in two signals shows that iron is present as two components [23]: (i) iron oxide nanoparticles (blue curve) corresponding to the small nanoparticles observed with TEM and (ii) Fe^{3+} ions (red curve) dispersed into the silica matrix.

3.2. Textural properties of xerogels

Textural properties of all the samples are given in Table 4. The nitrogen adsorption-desorption isotherms are represented in Figures 5 and 6 for Fe and Pd series respectively. All isotherms have similar shapes corresponding to a mixture of types I and II isotherms according to the BDDT classification [25], characterized by a sharp increase at low relative pressure followed by a plateau (type I, microporous solid) and at high pressure, the adsorbed volume increases quickly like in type II isotherm (macroporous solid). Samples present narrow hysteresis excepted for Fe/SiO_2-C sample where the hysteresis is more pronounced. So the presence of hysteresis on nitrogen adsorption-desorption isotherms corresponds to the presence of mesopores inside samples.

For the Fe series, the use of industrial grade reagents and the drying under ambient flowing air seem to not modify the texture of the samples as the isotherms keep a similar shape (Figure 5), only the hysteresis is reduced between Fe/SiO_2-C sample and the other two. The specific surface area stays similar at 230 m^2/g for Fe/SiO_2-C sample and 255 m^2/g for Fe/SiO_2-I2 sample.

For the Pd series, the use of industrial grade reagents and the drying under ambient flowing air seem to not modify the texture of the samples as the isotherms keep a similar shape (Figure 6) but this time, the specific surface area is modified from 370 to 250 m^2/g from Pd/SiO_2-C sample to Pd/SiO_2-I2 sample. For this series, the microporosity decreases slightly.

Under increasing mercury pressure (Figures 7 and 8), all samples present two successive behaviors: (i) at low pressure, samples collapse under the isostatic pressure; (ii) above a pressure of transition (P_t), the mercury enters into the pores of the samples [23]. This pressure (P_t) can be observed in the pressurization curve by a change of slope [23]. Two models are used to describe both phenomena and calculate the pore size distribution of mercury porosimetry [23]. The collapse of larger pores below P_t is described by Pirard's model [26], while mercury intrusion, above P_t, is described by Washburn's equation [26].

For the Fe series, the Fe/SiO_2-I1 and Fe/SiO_2-I2 samples present a smaller P_t, around 2-4 MPa, than Fe/SiO_2-C sample where P_t is around 32 MPa. Furthermore, the macroporous volume, V_{Hg}, is higher for Fe/SiO_2-I1 samples (4.2 cm^3/g) than the other two samples (3.2 and 3.5 cm^3/g).

For the Pd series, P_t is similar for the three samples, between 96 and 117 MPa. The macroporous volume, V_{Hg}, is higher for Pd/SiO_2-C sample (4.1 cm^3/g) compared to the other two samples(3.2-3.3 cm^3/g).

With nitrogen adsorption-desorption isotherms and mercury porosimetry measurements, it is possible to represent the cumulative volume distribution over the entire pore size [23]. All samples with iron and palladium are presented in Figure 9 and 10 respectively. These distributions were calculated by different methods applied to their respective validity domains: (i) for micropores, Brunauer's method was used; (ii) for mesopores smaller than 7.5 nm, Broekhoff-de-Boer's method was used; (iii) for pores larger than 7.5 nm, Pirard's and

Washburn's models were applied to mercury porosimetry results [22]. The total cumulative volume is V_T, which is obtained by addition of the specific pore volume obtained by mercury porosimetry (V_{Hg}), the cumulative volume of the pores whose size is included between 2 and 7.5 nm ($V_{cum<7.5nm}$) and the microporous pore volume determined by the Dubinin–Raduskevitch theory (V_{DR}) (Table 4).

All samples are characterized by a steep volume increase around 0.7-0.9 nm. In the range of meso- and macropores, one observes that all samples exhibit a broad distribution. These xerogels then contain micropores (width < 2 nm), mesopores (2 nm < width < 50 nm) and macropores (width > 50 nm). For the Fe series, the distribution shifts towards higher pores when the industrial conditions are used during the synthesis step (Fe/SiO_2-I1 and Fe/SiO_2-I2 samples in Figure 9). For the Pd samples, the distributions are quiet similar in all cases (Figure 10).

3.3. Hydrodechlorination activity of xerogel catalysts

For each pair of catalysts made with the same synthesis way, the hydrodechlorination activity is evaluated by using TCP in water. The different conditions used during the tests are presented in Table 2. The results with Fe/SiO_2-C & Pd/SiO_2-C samples are presented in Figure 11.

Without hydrogen, there is no degradation of TCP (see conditions in Table 2). In the presence of Fe/SiO_2-C + H_2, the TCP concentration does not decrease (Figure 11). Under Pd/SiO_2-C + H_2 and Pd/SiO_2-C + Fe/SiO_2-C + H_2 conditions, the TCP concentration decreases of about 80 % after 6 h and phenol appears under these conditions. Pd/SiO_2-C nanoparticles thus allow dechlorination of TCP but the phenol is then degraded only if the Fe/SiO_2 nanoparticles are present. Indeed, it is only in the condition Pd/SiO_2-C + Fe/SiO_2-C + H_2 that the phenol concentration decreases between 6 and 24 h from 13 to 1 ppm. In the Pd/SiO_2-C +

H_2 condition, the phenol concentration remains at 13 ppm. Similar evolutions are obtained for the other two pairs.

The TCP degradation is represented for the three pairs on Figure 12. Similar trends are observed: the concentration falls to zero after 24h and the concentration decreases rapidly during the first 6 h. The I1 condition leads to the faster degradation, degrading nearly 100 % after 6 h, while C condition and I2 condition reach 85 and 75 % of TCP degradation respectively.

The TOC measurements have been measured on samples from catalytic experiments with Pd/SiO_2 only and Pd/SiO_2 + Fe/SiO_2 catalyst tests (Table 5, after 24 h). These measurements coincided with Figure 11. Indeed, as observed on Figure 11, the catalytic experiment with Pd/SiO_2 only dechlorinated the TCP and produced phenol, so the TOC does not change very much (~ 94 % remaining, Table 5) as the TCP is converted in another organic compound. But when Fe/SiO_2 catalyst is combined with Pd/SiO_2, the complete mineralization is obtained (Table 5) as the dechlorinated phenol is totally degraded by iron catalyst.

4. Discussion

4.1. Composition and formation of xerogel catalysts: EDAS main factor for catalyst morphology

TEM micrographs, XRD patterns and Mössbauer spectroscopy allows to understand the composition of the samples. For the Pd-doped samples, they are composed of Pd nanoparticles of 2-3 nm dispersed in silica while, for Fe-doped samples, they are composed of iron oxide nanoparticles of 1-2 nm and Fe^{3+} ions dispersed in silica. This dispersion of metallic or metallic oxide nanoparticles is obtained thanks to EDAS [22,31,32]. This molecule is composed of an ethylene diamine group which complex metallic ions during synthesis. The complexed EDAS

molecule is more reactive that TEOS when forming silica, leading to the dispersion of metallic species nanoparticles inside silica matrix [22,31,32]. The nanoparticles stay accessible thanks to the porosity of silica and have high resistance to sintering and leaching [22,31,32].

The modification of synthesis parameters does not modify the composition and dispersion of nanoparticle inside silica. Indeed, the weight percentage of dopant stays constant in each series and the TEM micrographs are similar inside the series.

As observed in Table 1, in each series, the amount of reactants were identical. Previously [22,31,32], it was shown that the EDAS/TEOS ratio influences greatly the texture of silica catalyst. Indeed, EDAS plays a role of nucleating agent of silica particles due to its greater chemical reactivity than TEOS [22,31,32]. So, in a series, if the amount of EDAS increases, the silica particles decrease leading to larger specific surface area, S_{BET}. In this work, the ratio stays identical within the same series, the S_{BET} is so in the same rage within the series. Indeed for Fe-doped samples, similar textural properties are obtained as in [23] where the Fe/SiO_2 samples had S_{BET} value between 200-400 m^2/g, similar adsorption-desorption isotherms were measured. For Pd series also similar textural properties are obtained as in [22,31] where the specific surface areas were between 300-500 m^2/g.

The use of industrial grade reactants and drying conditions under ambient air do not modify greatly the catalysts texture as observed in Figures 5, 6 and Table 4. Indeed, previously, it was shown for $Pd\text{-}Ag/SiO_2$ catalysts [15] that the use of industrial grade reactants kept textural properties of the catalysts.

4.2. Catalytic activity of xerogels: Role of each catalyst

From the catalytic tests, the role of each catalyst can be deduce: the Pd/SiO_2 catalysts allow to dechlorinate the TCP while the Fe/SiO_2 catalysts allows to degrade the phenol. The two catalysts are necessary to degrade the TCP.

Indeed, it was shown [9] that Pd/SiO_2 catalysts can dechlorinate molecules. Noble metal catalysts (Group VIII) are very active for the hydrodechlorination reaction [1,2,14,33], the dechlorination of TCP with Pd catalyst has been shown previously [12] leading to phenol formation. In this case, hydrogen is dissociatively absorbed onto reducing catalyst (Pd) to form a metal hydride (M–H) [7], which in turn dechlorinates the target substrate. But it remains phenol that needs to be degraded. Iron catalyst allows to eliminate phenol (Figures 11 and 12, Table 5). Indeed, without Fe/SiO_2 catalysts no degradation happens as phenol concentration stays constant (Figure 11). The phenol degradation mechanism can be due photo-Fenton effect of this catalyst [23,34]. Indeed, the tests are made in glass vessels under visible light, in this case radical production can be obtained thanks to equation (3) due to Fe^{3+} complex [35]. In these tests, the Fe/SiO_2 catalysts are composed of Fe^{3+} species which can act as equation (3) [23].

$$Fe^{3+}(L)_n + h\nu \rightarrow Fe^{2+}(L)_{n-1} + L_{ox}^{\bullet} \quad (3)$$

where L is a ligand, $L_{ox}^{\bullet}$ is an oxidized ligand, h is the Planck constant ($6{,}63 * 10^{-34}$ J.s) and ν is the light frequency (Hz) [35].

The complete degradation of TCP is then possible due to two different mechanisms: hydrodechlorination with Pd/SiO_2 catalyst and photo-Fenton phenol degradation with Fe/SiO_2 catalyst. The TOC measurements ensured that a complete mineralization is obtained with all binary catalyst couples (Table 5).

For each series, the modification of the synthesis parameters (drying and reactants grades) does not modify greatly the activity of the catalysts as all pairs are able to degrade the TCP within 24 h as depicted on Figure 12. The simplification of the catalyst synthesis towards industrial scale is then possible giving similar results as laboratory catalysts.

5. Conclusions

In this work, Pd/SiO_2 and Fe/SiO_2 catalysts were synthesized by the cogelation process in order to obtain a binary catalyst efficient for the total degradation of chlorinated compounds and that can be produced at industrial scale.

Concerning the synthesis, the method has been adapted to produce a synthesis closer to industrial conditions. Two major modifications were made: the use of industrial grade reactants and the use of ambient air drying to replace the costly vacuum drying. These modifications led to the production of three catalyst couples: laboratory scale condition samples, industrial grades samples with vacuum drying and industrial grades samples with ambient air drying.

The binary catalysts have been characterized to assess the impact of the synthesis condition modifications. It results that in all cases, similar couples are obtained with palladium nanoparticles dispersed in porous silica for the Pd/SiO_2 samples and iron oxide nanoparticles dispersed in porous silica for the Fe/SiO_2 samples. Good dispersion of the metallic species is observed in each sample thanks to the use of EDAS as complexing molecule of metallic precursor.

The binary catalysts are then tested on the degradation of TCP in water medium. Each couple shows a complete degradation of the molecule thanks to the coupled action of the two catalysts: Pd allows the dechlorination of TCP into phenol and Fe allows phenol degradation with photo-Fenton reaction.

The industrial synthesis conditions allow to obtain a very efficient binary catalyst with similar physico-chemical and catalytic properties as laboratory scale conditions samples.

Acknowledgments

S. D. L. thanks to the Belgian National Funds for Scientific Research (F.R.S.-FNRS) for her Associate Senior Researcher position. The authors are grateful to Prof. Benoît Heinrichs from the University of Liège for fruitful discussions. The Ministère de la Région Wallonne Direction Générale des Technologies, de la Recherche et de l'Energie (DG06) (NANOMICRO project n° 6917, GREENWIN Pole), the Fonds de Recherche Fondamentale Collective and the Fonds de Bay are gratefully acknowledged.

Conflict of interest

The authors declare that there is no conflict of interest concerning this work.

References

[1] C.B. Molina, A.H. Pizarro, J.A. Casas, J.J. Rodriguez, Aqueous-phase hydrodechlorination of chlorophenols with pillared clays-supported Pt, Pd and Rh catalysts, Appl. Catal. B Environ. 148–149 (2014) 330–338. doi:10.1016/j.apcatb.2013.11.010.

[2] W. Chang, H. Kim, G.Y. Lee, B.J. Ahn, Catalytic hydrodechlorination reaction of chlorophenols by Pd nanoparticles supported on graphene, Res. Chem. Intermed. 42 (2016) 71–82. doi:10.1007/s11164-015-2368-8.

[3] X. Ma, Z. Sun, X. Hu, Electrocatalytic dechlorination of chlorophenols on palladium/graphene-Nafion/titanium mesh electrode, J. Water Process Eng. 26 (2018) 72–82. doi:10.1016/j.jwpe.2018.09.008.

[4] P.J. Dorathi, P. Kandasamy, Dechlorination of chlorophenols by zero valent iron impregnated silica, J. Environ. Sci. 24 (2012) 765–773. doi:10.1016/S1001-0742(11)60817-6.

[5] Y.R. Wang, W. Chu, Photo-assisted degradation of 2,4,5-trichlorophenol by Electro-Fe(II)/Oxone® process using a sacrificial iron anode: Performance optimization and reaction mechanism, Chem. Eng. J. 215–216 (2013) 643–650. doi:10.1016/j.cej.2012.11.042.

[6] G. Collins, C. Foy, S. McHugh, V. O'Flaherty, Anaerobic treatment of 2,4,6-trichlorophenol in an expanded granular sludge bed-anaerobic filter (EGSB-AF) bioreactor at 15°C, FEMS Microbiol. Ecol. 53 (2005) 167–178. doi:10.1016/j.femsec.2004.10.008.

[7] U.D. Patel, S. Suresh, Dechlorination of chlorophenols using magnesium-palladium bimetallic system, J. Hazard. Mater. 147 (2007) 431–438. doi:10.1016/j.jhazmat.2007.01.029.

[8] T. Zhou, Y. Li, T.T. Lim, Catalytic hydrodechlorination of chlorophenols by Pd/Fe nanoparticles: Comparisons with other bimetallic systems, kinetics and mechanism, Sep. Purif. Technol. 76 (2010) 206–214. doi:10.1016/j.seppur.2010.10.010.

[9] S. Lambert, F. Ferauche, A. Brasseur, J.P. Pirard, B. Heinrichs, Pd-Ag/SiO2 and Pd-Cu/SiO2 cogelled xerogel catalysts for selective hydrodechlorination of 1,2-dichloroethane into ethylene, Catal. Today. 100 (2005) 283–289. doi:10.1016/j.cattod.2004.08.015.

[10] S.L. Pirard, J.G. Mahy, J.-P. Pirard, B. Heinrichs, L. Raskinet, S.D. Lambert, Development by the sol-gel process of highly dispersed Ni-Cu/SiO2 xerogel catalysts for selective 1,2-dichloroethane hydrodechlorination into ethylene, Microporous Mesoporous Mater. 209 (2015). doi:10.1016/j.micromeso.2014.08.015.

[11] J.G. Mahy, V. Claude, L. Sacco, S.D. Lambert, Ethylene polymerization and hydrodechlorination of 1,2-dichloroethane mediated by nickel(II) covalently anchored

to silica xerogels, J. Sol-Gel Sci. Technol. 81 (2017). doi:10.1007/s10971-016-4272-0.

[12] X. Cui, W. Zuo, M. Tian, Z. Dong, J. Ma, Highly efficient and recyclable Ni MOF-derived N-doped magnetic mesoporous carbon-supported palladium catalysts for the hydrodechlorination of chlorophenols, J. Mol. Catal. A Chem. 423 (2016) 386–392. doi:10.1016/j.molcata.2016.07.041.

[13] M. Munoz, Z.M. de Pedro, J.A. Casas, J.J. Rodriguez, Chlorophenols breakdown by a sequential hydrodechlorination-oxidation treatment with a magnetic Pd-Fe/g-Al2O3 catalyst, Water Res. 47 (2013) 3070–3080.

[14] J.W. Bozzelli, Y. Chen, S. Chuang, 1,2-Dichloroethane and Trichloroethylene over Rh/SiO2 catalysts, Chem. Eng. Comm. 115 (1992) 1–11.

[15] S. Lambert, F. Ferauche, B. Heinrichs, N. Tcherkassova, J.P. Pirard, C. Alié, Methods for the preparation of bimetallic xerogel catalysts designed for chlorinated wastes processing, J. Non. Cryst. Solids. 352 (2006) 2751–2762. doi:10.1016/j.jnoncrysol.2006.03.055.

[16] G.S. Pozan, I. Boz, Hydrodechlorination of 2,3,5-Trichlorophenol in Methanol/Water on Carbon Supported Pd-Rh Catalysts, Environ. Eng. Sci. 25 (2008) 1197–1202. doi:10.1097/PAS.0000000000000530.

[17] E.J. Shin, M.A. Keane, Detoxifying chlorine rich gas streams using solid supported nickel catalysts, J. Hazard. Mater. 66 (1999) 265–278. doi:10.1016/S0304-3894(99)00003-5.

[18] X. Wang, M. Zhu, H. Liu, J. Ma, F. Li, Modificiation of Pd-Fe nanoparticles for catalytic dechlorination of 2,4-dichlorophenol, Sci. Total Environ. 449 (2013) 157–167.

[19] J.G. Mahy, L. Tasseroul, M. Herlitschke, R.P. Hermann, S.D. Lambert, Fe^{3+}/Iron Oxide/SiO2 Xerogel Catalysts for p-nitrophenol Degradation by Photo-Fenton Effects: Influence of Thermal Treatment on Catalysts Texture, in: Mater. Today Proc., 2016. doi:10.1016/j.matpr.2016.01.043.

[20] J.J. Reinosa, C. María, Á. Docio, V.Z. Ramírez, Hierarchical nano ZnO-micro TiO_2 composites : High UV protection yield lowering photodegradation in sunscreens, Ceram. Int. 44 (2018) 2827–2834. doi:10.1016/j.ceramint.2017.11.028.

[21] G.L.-M. Léonard, C.A. Pàez, A.E. Ramírez, J.G. Mahy, B. Heinrichs, Interactions between Zn^{2+} or ZnO with TiO_2 to produce an efficient photocatalytic, superhydrophilic and aesthetic glass, J. Photochem. Photobiol. A Chem. 350 (2018). doi:10.1016/j.jphotochem.2017.09.036.

[22] S. Lambert, C. Alié, J.P. Pirard, B. Heinrichs, Study of textural properties and nucleation phenomenon in Pd/SiO2, Ag/SiO2 and Cu/SiO2 cogelled xerogel catalysts, J. Non. Cryst. Solids. 342 (2004) 70–81. doi:10.1016/j.jnoncrysol.2004.06.005.

[23] J.G. Mahy, L. Tasseroul, A. Zubiaur, J. Geens, M. Brisbois, M. Herlitschke, et al., Highly dispersed iron xerogel catalysts for p-nitrophenol degradation by photo-Fenton effects, Microporous Mesoporous Mater. 197 (2014) 164–173. doi:10.1016/j.micromeso.2014.06.009.

[24] G.W. Brinker, C. Jeffrey, Scherer, Sol-gel science: the physics and chemistry of sol-gel processing, Academic presse, San Diego, 2013.

[25] A. Lecloux, Exploitation des isothermes d'adsorption et de désorption d'azote pour l'étude de la texture des solides poreux, Mémoires Société R. Des Sci. Liège. (1971) 169–209.

[26] R. Pirard, B. Heinrichs, O. Van Cantfort, J.P. Pirard, Mercury Porosimetry Applied to Low Density Xerogels; Relation between Structure and Mechanical Properties, J. Sol-Gel Sci. Technol. 13 (1998) 335–339. doi:10.1023/A:1008676211157.

[27] J.G. Mahy, S.D. Lambert, G.L.-M. Léonard, A. Zubiaur, P.-Y. Olu, A. Mahmoud, et al., Towards a large scale aqueous sol-gel synthesis of doped TiO2: Study of various metallic dopings for the photocatalytic degradation of p-nitrophenol, J. Photochem. Photobiol. A Chem. 329 (2016). doi:10.1016/j.jphotochem.2016.06.029.

[28] A. L. Patterson, The Scherrer Formula for X-Ray Particle Size Determination, Phys. Rev. 56 (1939) 978–982. doi:10.1103/PhysRev.56.978.

[29] C.M. Malengreaux, S. Douven, D. Poelman, B. Heinrichs, J.R. Bartlett, An ambient temperature aqueous sol–gel processing of efficient nanocrystalline doped TiO2-based photocatalysts for the degradation of organic pollutants, J. Sol-Gel Sci. Technol. 71 (2014) 557–570. doi:10.1007/s10971-014-3405-6.

[30] C.M. Malengreaux, G.M.-L. Léonard, S.L. Pirard, I. Cimieri, S.D. Lambert, J.R. Bartlett, et al., How to modify the photocatalytic activity of TiO2 thin films through their roughness by using additives. A relation between kinetics, morphology and synthesis, Chem. Eng. J. 243 (2014) 537–548. doi:10.1016/j.cej.2013.11.031.

[31] S. Lambert, J.-F. Polard, J.-P. Pirard, B. Heinrichs, Improvement of metal dispersion in Pd/SiO2 cogelled xerogel catalysts for 1,2-dichloroethane hydrodechlorination, Appl. Catal. B 50 (2004) 127-140.

[32] C. Alié, S.D. Lambert, B. Heinrichs, J. Pirard, Nucleation Phenomenon in Silica Xerogels and Pd/SiO2 , Ag/SiO2 , Cu/SiO2 Cogelled Catalysts, J. Sol-Gel Sci. Technol. 26 (2003) 827–830.

[33] G.N. Jovanovic, J.E. Atwater, P. Žnidaršič-Plazl, I. Plazl, Dechlorination of polychlorinated phenols on bimetallic Pd/Fe catalyst in a magnetically stabilized fluidized bed, Chem. Eng. J. 274 (2015) 50–60. doi:10.1016/j.cej.2015.03.087.

[34] V. Kavitha, K. Palanivelu, The role of ferrous ion in Fenton and photo-Fenton processes for the degradation of phenol, Chemosphere. 55 (2004) 1235–1243. doi:10.1016/j.chemosphere.2003.12.022.

[35] J.J. Pignatello, E. Oliveros, A. MacKay, Advanced oxidation processes for organic contaminant destruction based on the fenton reaction and related chemistry, Crit. Rev. Environ. Sci. Technol. 36 (2006) 1–84. doi:10.1080/10643380500326564.

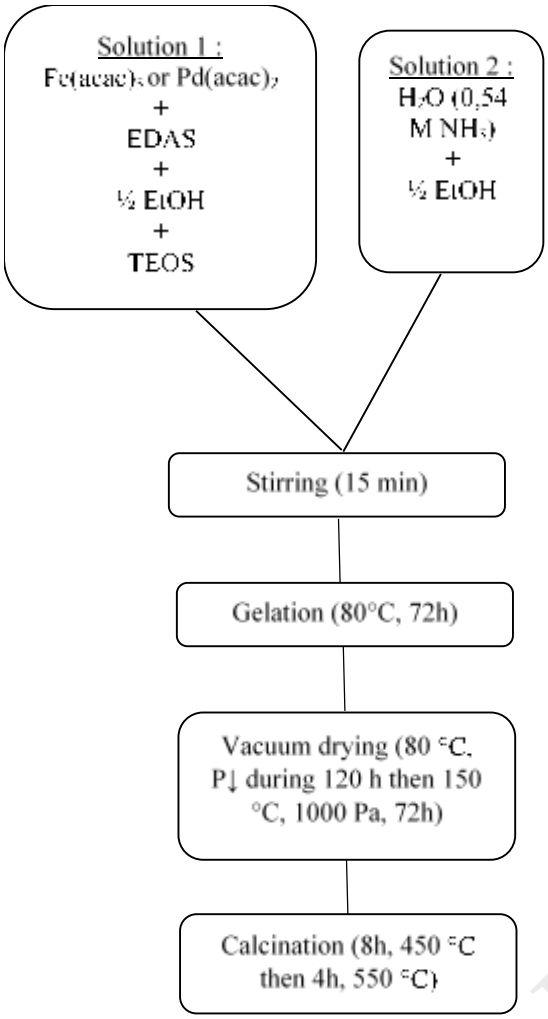

Figure 1: Scheme of the "classical" synthesis at laboratory scale

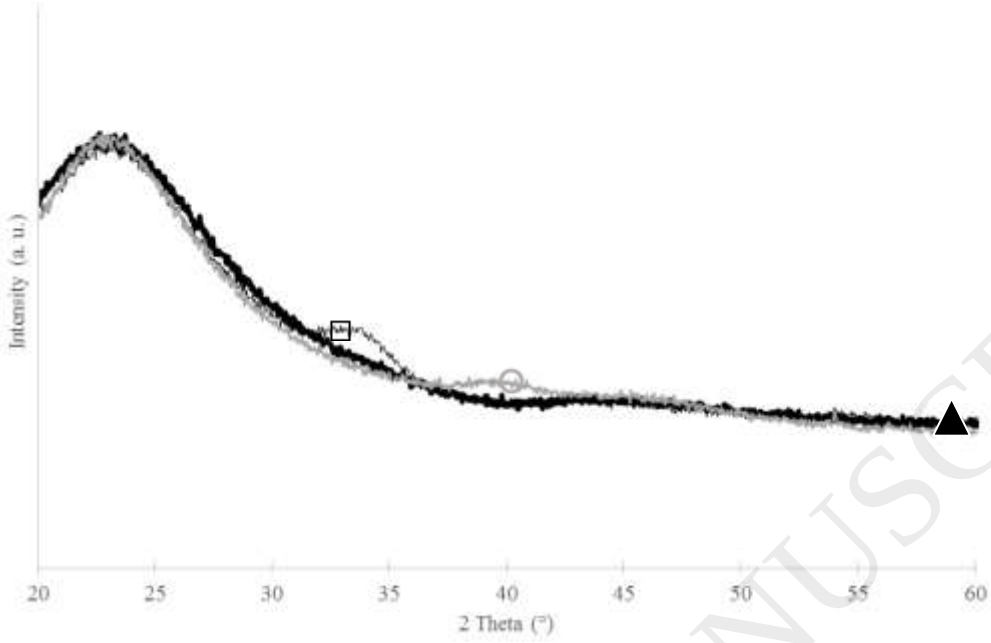

Figure 2: XRD patterns of (▲) Fe/SiO_2-I2, (□) Pd/SiO_2-I2 calcined and (○) Pd/SiO_2-I2 reduced samples.

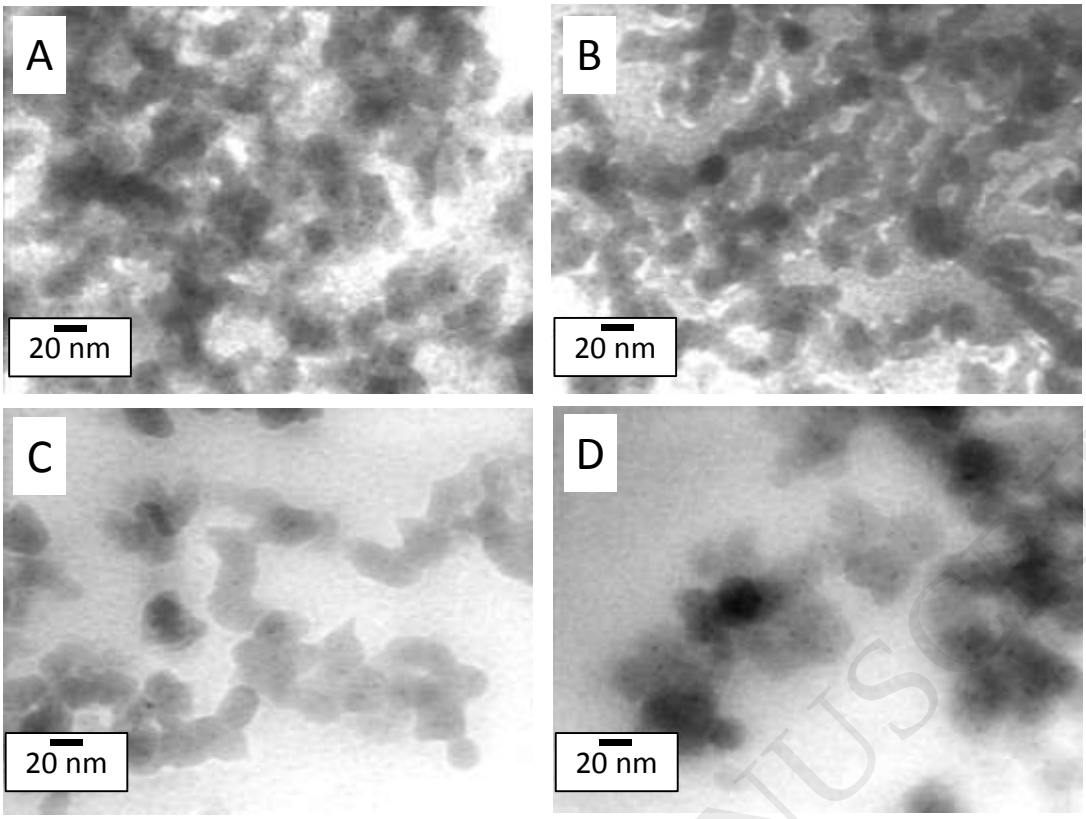

Figure 3: TEM micrographs of (A) Fe/SiO_2-C, (B) Fe/SiO_2-I2, (C) Pd/SiO_2-C and (D) Pd/SiO_2-I2 samples.

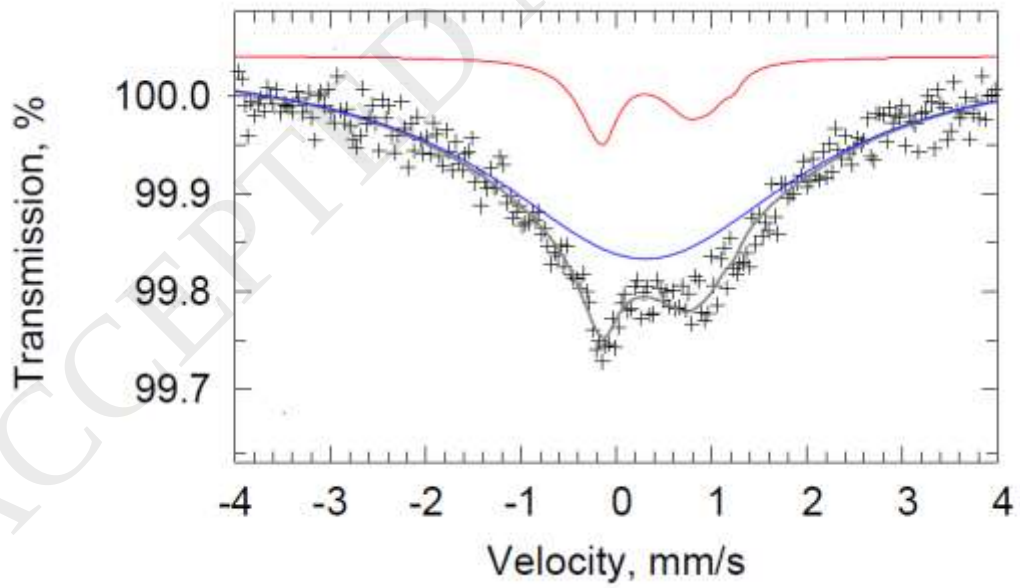

Figure 4: Transmission iron-57 Mössbauer spectrum of Fe/SiO_2-I2 sample.

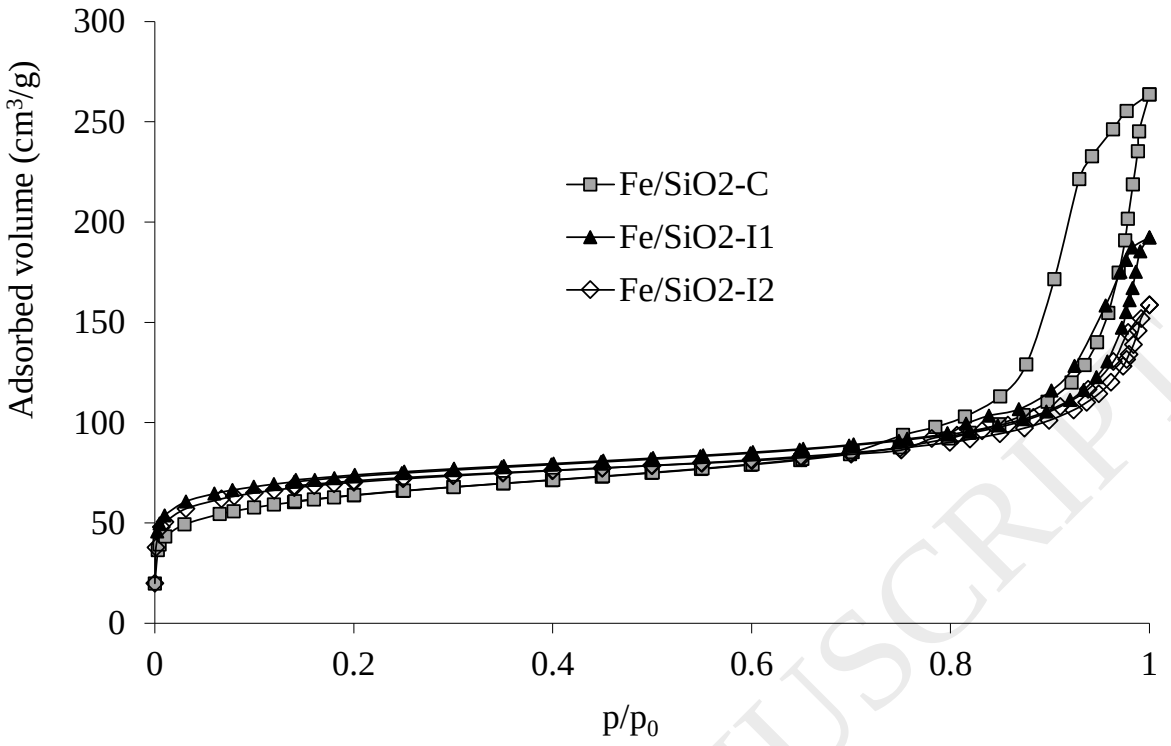

Figure 5: Nitrogen adsorption-desorption isotherms of (■) Fe/SiO_2-C, (▲) Fe/SiO_2-I1, and (◊) Fe/SiO_2-I2 samples.

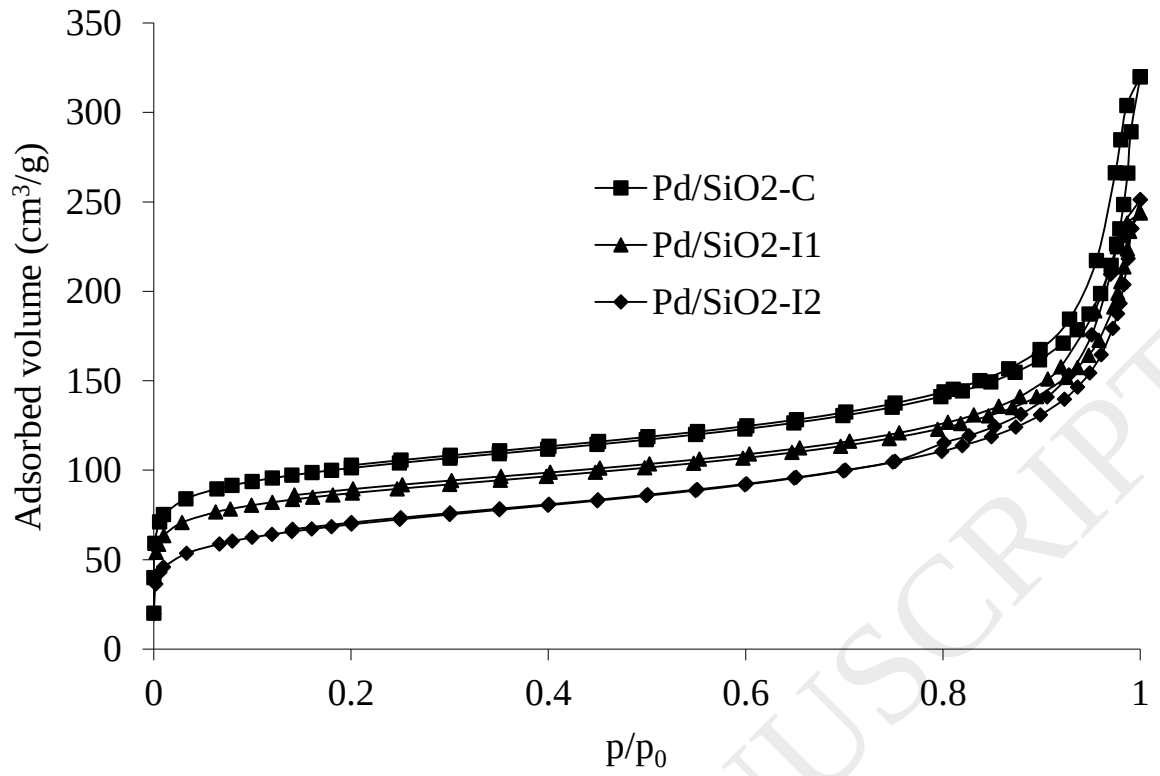

Figure 6: Nitrogen adsorption-desorption isotherms of (■) Pd/SiO_2-C, (▲) Pd/SiO_2-I1, and (⧫) Pd/SiO_2-I2 samples.

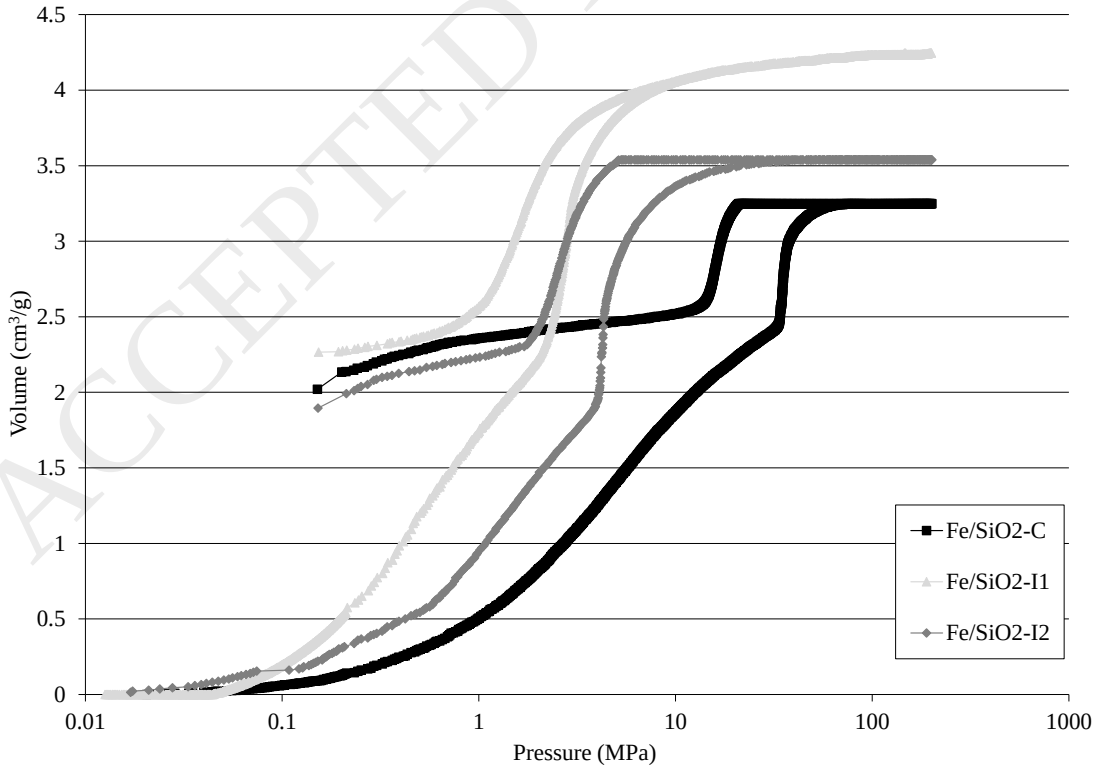

Figure 7: Mercury porosimetry curves of (■) Fe/SiO_2-C, (▲) Fe/SiO_2-I1, and (⧫) Fe/SiO_2-I2 samples.

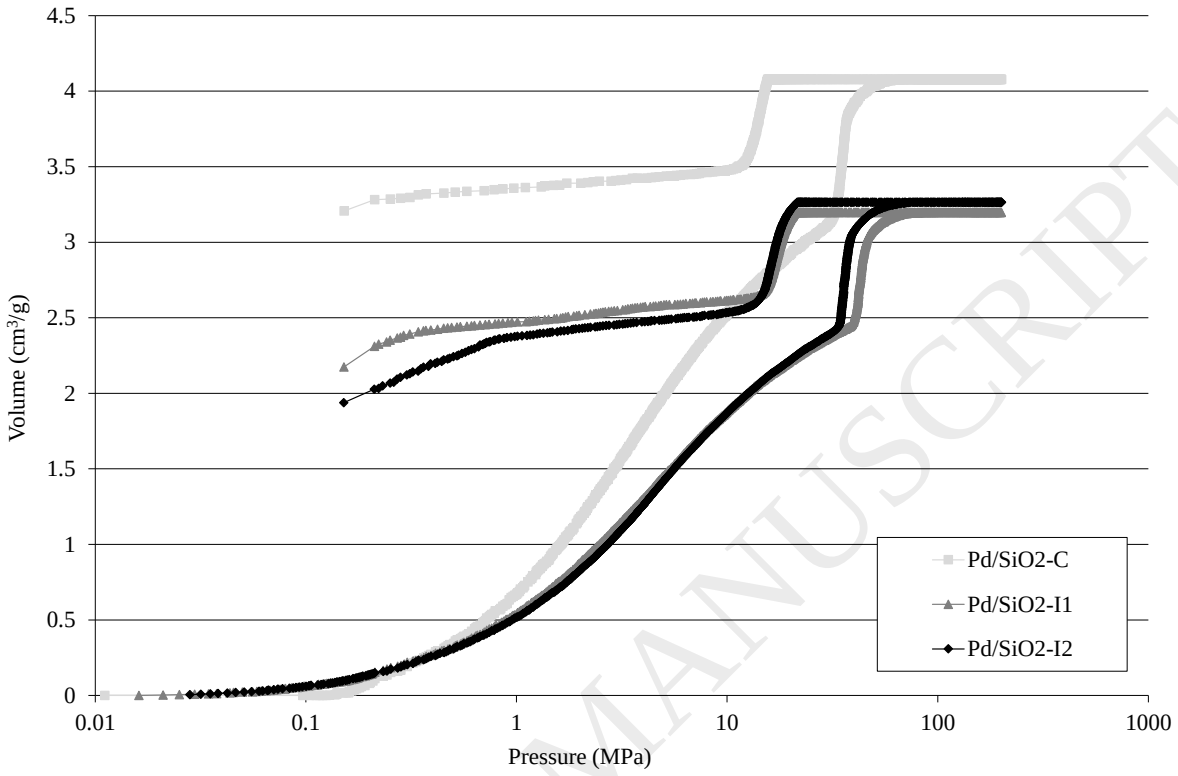

Figure 8: Mercury porosimetry curves of (■) Pd/SiO_2-C, (▲) Pd/SiO_2-I1, and (⧫) Pd/SiO_2-I2 samples.

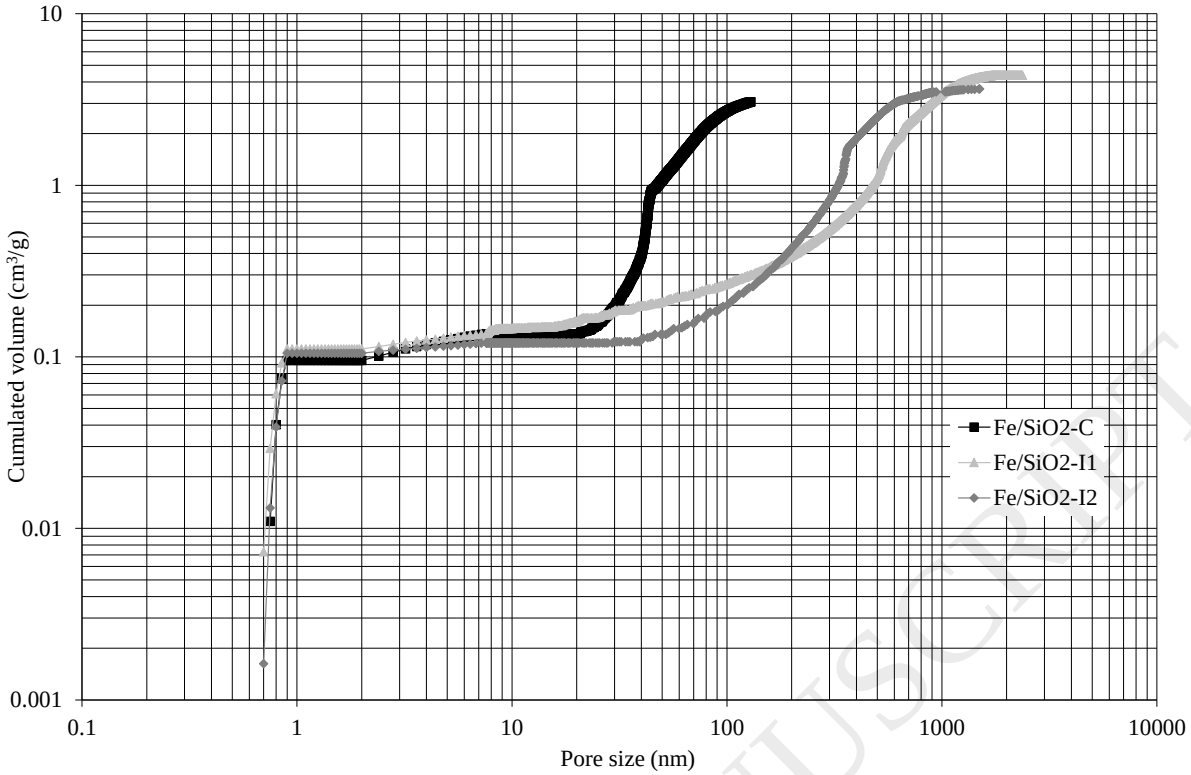

Figure 9: Pore size distributions of (■) Fe/SiO_2-C, (▲)Fe/SiO_2-I1, and (⧫) Fe/SiO_2-I2 samples.

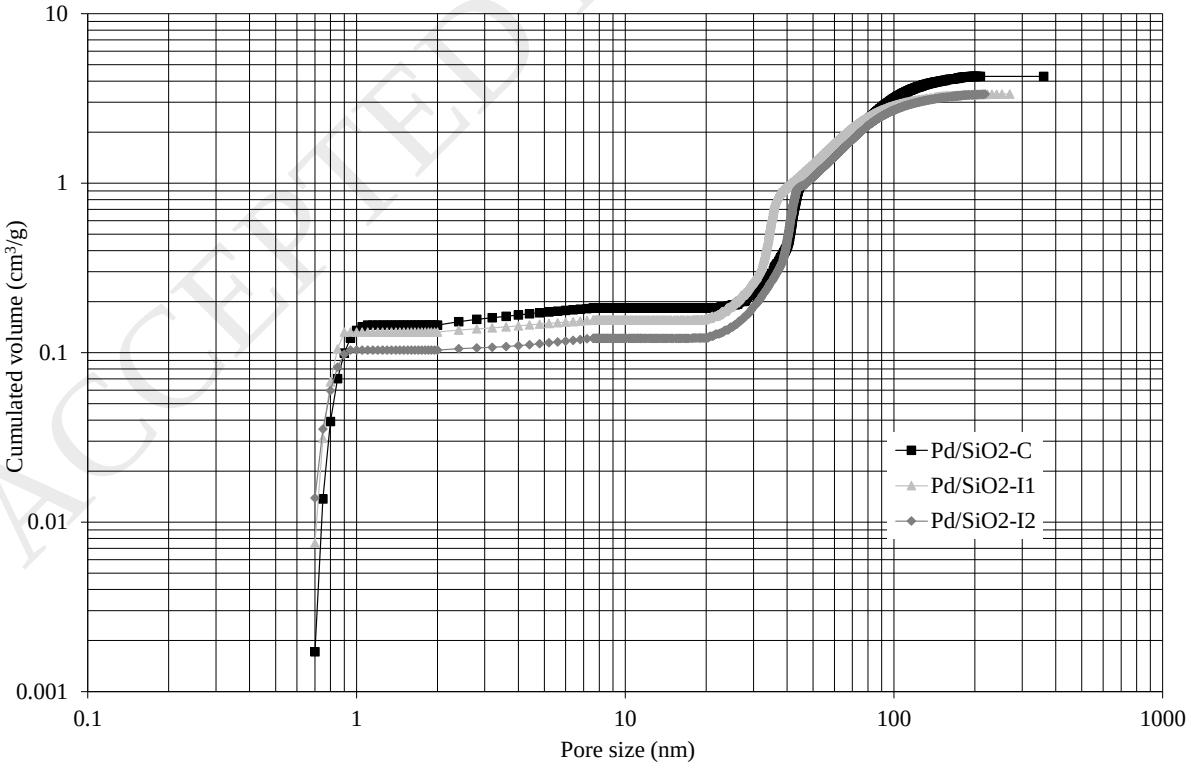

Figure 10: Pore size distributions of (■) Pd/SiO_2-C, (▲) Pd/SiO_2-I1, and (⧫) Pd/SiO_2-I2 samples.

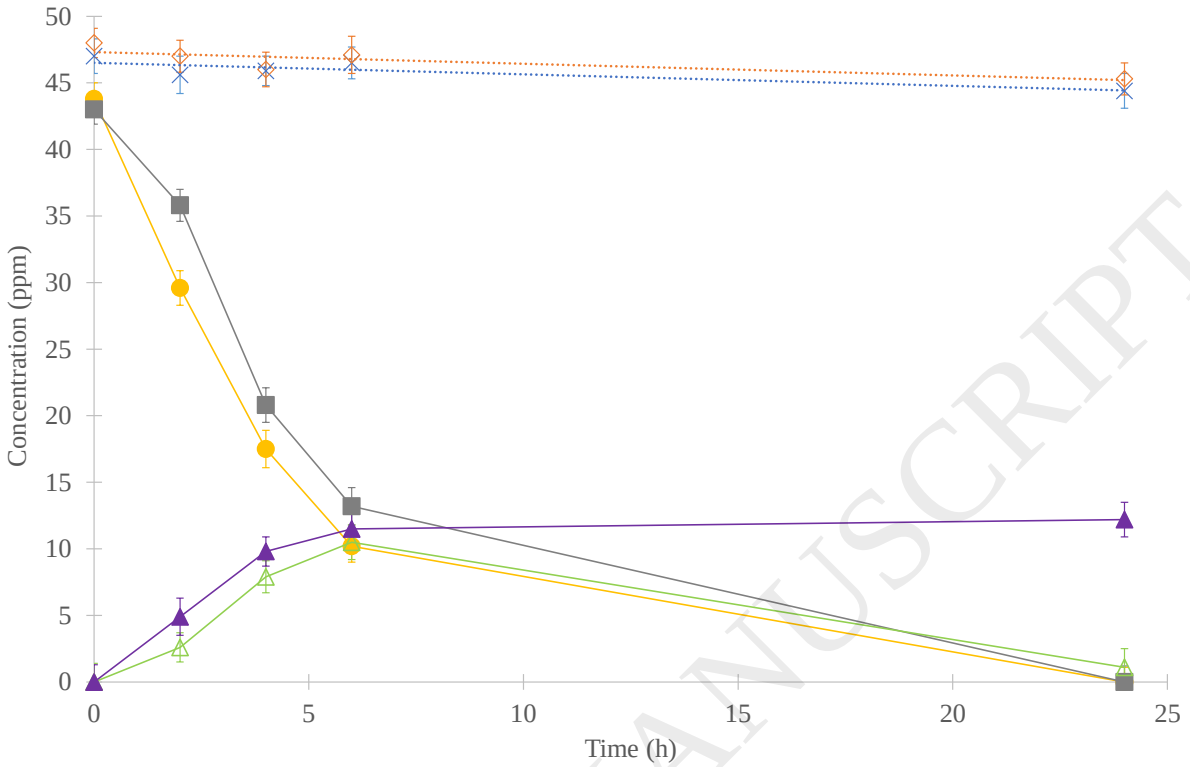

Figure 11: Degradation of *2,4,6*-tricholorophenol with Fe/SiO_2-C (10^{-4} M), Pd/SiO_2-C (10^{-5} M) and H_2. Conditions of Table 2 are represented: (×) H_2 only (T+ condition); (◊) Fe/SiO_2-C + H_2; (■) Pd/SiO_2-C + H_2; (●) Fe/SiO_2-C + Pd/SiO_2-C + H_2; (▲) [Phenol] in condition Pd/SiO_2-C + H_2; (△) [Phenol] in condition Fe/SiO_2-C + Pd/SiO_2-C + H_2.

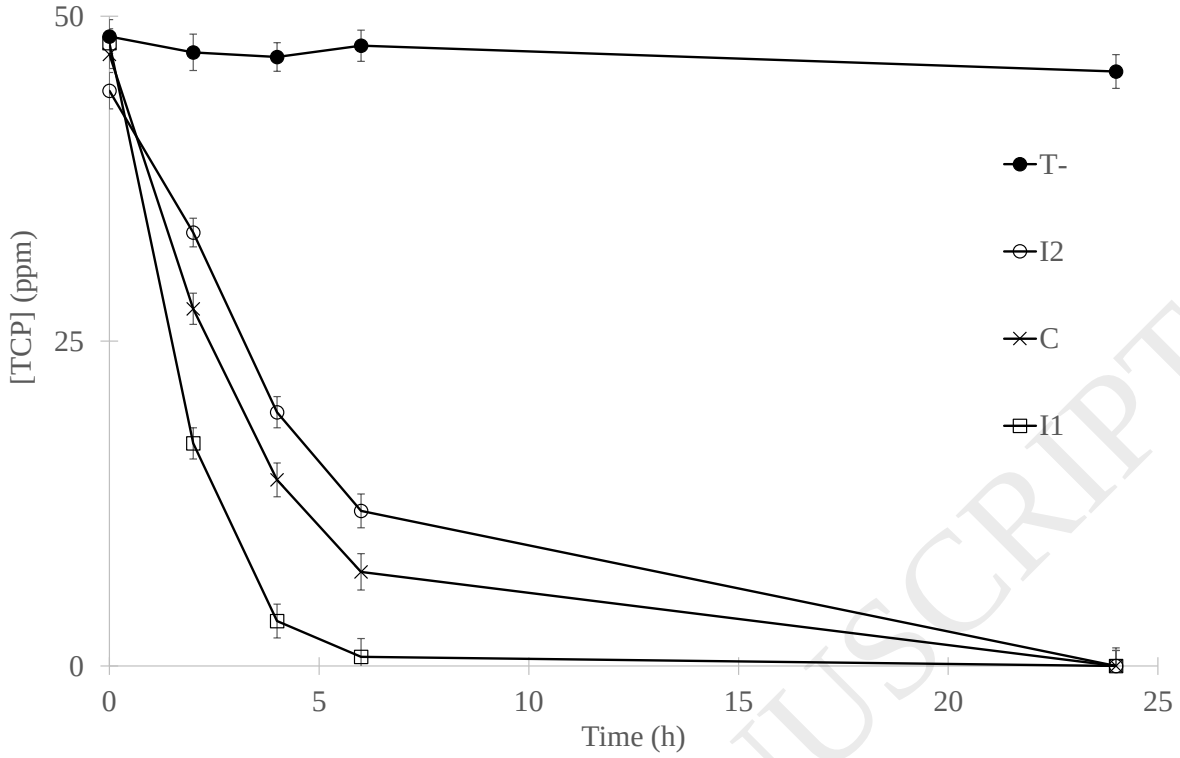

Figure 12: Degradation of *2,4,6*-tricholorophenol (TCP) under H_2 with (×) Fe/SiO_2-C & Pd/SiO_2-C couple, (□) Fe/SiO_2-I1 & Pd/SiO_2-I1 couple and (○) Fe/SiO_2-I2 & Pd/SiO_2-2 couple. (●) T- corresponds to the condition with only TCP.

Table 1: Synthesis operating variables

Sample	Ethanol (mmol)	TEOS or Dynasil (mmol)	EDAS or Dynasilan DAMO (mmol)	Water (mmol)	EDAS/TEOS	$Fe(acac)_3$ (mmol)	$Pd(acac)_2$ (mmol)	Theoretical metal loading (wt%)	Actual metal loading[a] (wt%)
Fe/SiO_2-C	2570	249	8.37	1274	0.033	2.79	-[b]	1.0	1.0
Fe/SiO_2-I1	2570	249	8.37	1274	0.033	2.79	-[b]	1.0	0.9
Fe/SiO_2-I2	2570	249	8.37	1274	0.033	2.79	-[b]	1.0	1.0
Pd/SiO_2-C	2570	253	2.92	1280	0.012	-[b]	1.46	1.0	1.0
Pd/SiO_2-I1	2570	253	2.92	1280	0.012	-[b]	1.46	1.0	1.0
Pd/SiO_2-I2	2570	253	2.92	1280	0.012	-[b]	1.46	1.0	0.9

[a] measured by ICP-AES; -[b]: not present.

Table 2: conditions for hydrodechlorination test

Condition name	TCP 50 ppm	Fe/SiO_2 10^{-4} M	Pd/SiO_2 10^{-5} M	H_2
T -	✓	×	×	×
T +	✓	×	×	✓
TCP + Fe/SiO_2	✓	✓	×	×
TCP + Fe/SiO_2 + H_2	✓	✓	×	✓
TCP + Pd/SiO_2	✓	×	✓	×
TCP + Pd/SiO_2 + H_2	✓	×	✓	✓
TCP + Fe/SiO_2 + Pd/SiO_2	✓	✓	✓	×
TCP + Fe/SiO_2 + Pd/SiO_2 + H_2	✓	✓	✓	✓

✓ = present; × = not present; TCP = *2,4,6*-trichlorophenol.

Table 3. **Sizes of iron oxide, palladium and silica nanoparticles**

.

Sample	d_{Fe} (nm)	σ_{Fe} (nm)	d_{Pd} (nm)	σ_{Pd} (nm)	d_{SiO2} (nm)	σ_{SiO2} (nm)	d_{XRD} (nm)
Fe/SiO_2-C	1.3	0.3	-[a]	-[a]	23	5	-[a]
Fe/SiO_2-I1	1.6	0.3	-[a]	-[a]	24	4	-[a]
Fe/SiO_2-I2	1.4	0.2	-[a]	-[a]	22	4	-[a]
Pd/SiO_2-C	-[a]	-[a]	2.7	0.2	22	3	2
Pd/SiO_2-I1	-[a]	-[a]	2.5	0.2	23	4	2
Pd/SiO_2-I2	-[a]	-[a]	2.7	0.3	29	2	3

d_{Fe} = mean diameter of iron oxide particles measured by TEM ; σ_{Fe} = standard deviation associated with d_{Fe} ; d_{Pd} = mean diameter of metallic palladium particles measured by TEM ; σ_{Pd} = standard deviation associated with d_{Pd} ; d_{SiO2} = mean diameter of silica particles measured by TEM ; σ_{SiO2} = standard deviation associated with d_{SiO2}; d_{XRD} = crystallite size calculated by Scherrer equation ; -[a] = not present.

Table 4 : Sample textural properties

Sample	ρ_{app} (g cm^{-3}) ± 0.01	S_{BET} (m^2 g^{-1}) ± 5	S_{BdB} (m^2 g^{-1}) ±5	V_P (cm^3 g^{-1}) ± 0.1	V_{DR} (cm^3 g^{-1}) ± 0.01	$V_{cum<7.5nm}$ (cm^3 g^{-1}) ±0.01	V_{Hg} (cm^{3}g^{-1}) ±0.1	P_t (MPa)	k ($nm\ MPa^{0.25}$)	V_T (cm^3 g^{-1}) ±0.1
Fe/SiO_2-C	2.18	230	145	0.4	0.09	0.04	3.2	32	111	3.4
Fe/SiO_2-I1	2.16	265	65	0.3	0.11	0.03	4.2	2	793	4.4
Fe/SiO_2-I2	2.19	255	140	0.2	0.10	0.02	3.5	4	540	3.6
Pd/SiO_2-C	2.09	370	190	0.5	0.15	0.04	4.1	30	117	4.3
Pd/SiO_2-I1	2.10	310	125	0.4	0.13	0.02	3.2	39	96	3.4
Pd/SiO_2-I2	2.08	250	71	0.4	0.10	0.02	3.3	32	111	3.4

-[a] : not measured; ρ_{app} : apparent density measured by helium pycnometry; S_{BET} : specific surface area determined by the BET method; S_{BdB} : specific mesopore surface area determined by the Broekhoff–de Boer theory; V_p : specific liquid volume adsorbed at the saturation pressure of nitrogen; V_{DR} : specific micropore volume determined by the Dubinin–Raduskevitch theory; $V_{cum<7.5nm}$: cumulative volume pores of diameter between 2 and 7,5 nm determined by Broekhoff-de-Boer theory; V_{Hg} : specific pore volume measured by mercury porosimetry; P_t : pressure of change of mechanism during mercury porosimetry (change from collapse to intrusion) ; k : buckling model constant; V_T : pore volume obtained by addition of V_{DR}, $V_{cum<7.5nm}$ and V_{Hg}.

Table 5: TOC measurements after catalytic experiments (24 h)

Catalytic experiments	**Remaining organic carbon (%) ± 1**
TCP + Pd/SiO_2-C + H_2	94
TCP + Pd/SiO_2-I1 + H_2	93
TCP + Pd/SiO_2-I2 + H_2	95
TPC + Pd/SiO_2-C + Fe/SiO_2-C + H_2	2
TPC + Pd/SiO_2-I1 + Fe/SiO_2-I1 + H_2	0
TPC + Pd/SiO_2-I2 + Fe/SiO_2-I2 + H_2	3

The remaining organic carbon is calculated from the TOC measurement before and after the catalytic experiment = $\frac{TOC_{inital} - TOC_{final}}{TOC_{Initial}} * 100$